PRECLINICAL AND CLINICAL IMAGING – Note

Magnetic Resonance in Medicine 66:244–247 (2011)

16 T Diffusion Microimaging of Fixed Prostate Tissue: Preliminary Findings

Roger Bourne,[1]* Nyoman Kurniawan,[2] Gary Cowin,[3] Paul Sved,[4] and Geoff Watson[5]

Diffusion tensor microimaging was used to investigate the water diffusion properties of formalin-fixed prostate tissue at spatial resolution approaching the cellular scale. Diffusion tensor microimaging was performed at 16.4 T with 40 μm isotropic voxels. Diffusion tensor microimaging clearly demonstrated distinct microscopic diffusion environments and tissue architecture consistent with that seen on light microscopy of the same tissue. The most restricted diffusion environment is the secretory epithelial cell layer (voxel bulk mean diffusivity, $D = 0.4 \pm 0.1 \times 10^{-3}$ mm^2/sec). Diffusion in the fibromuscular stromal matrix is relatively less restricted ($D = 0.7 \pm 0.1 \times 10^{-3}$ mm^2/sec). In tumor tissue (Gleason pattern 4+4) distinct glandular and ductal structures are absent in the diffusion-weighted images and diffusivity is low ($D = 0.5 \pm 0.1 \times 10^{-3}$ mm^2/sec). Distinct stromal and epithelial diffusion compartments are the most likely origin of biexponential diffusion decay observed in vivo. Magn Reson Med 66:244–247, 2011.

Key words: diffusion; microimaging; prostate; DTI

Since prostate cancer is defined by tissue structure seen at histopathology, a detection method that generates contrast based on microscopic tissue structural properties would be expected to provide both sensitive and specific cancer detection to the extent that the contrast can be made to reflect the structures that define pathology. Diffusion-weighted water imaging (DWI) is an obvious candidate for this purpose because the free diffusion of water in tissue is known to be constrained by intra- and extra-cellular structures and cell walls. In contrast to T_1 and T_2 weighted imaging diffusion-weighted water imaging can reveal both the scale and orientation of tissue structure because diffusion-weighted water imaging contrast depends on the net diffusion of water over a specific time period in a specific direction. Two parameters are commonly used to describe the rate and spatial freedom of water diffusion—apparent self-diffusion coefficient (ADC) and the fractional anisotropy (FA), respectively (1). However, in response to inconsistent reported definitions of apparent self-diffusion coefficient, Basser and Jones (1) have recommended the preferential use of the bulk mean diffusivity (D, derived from diffusion tensor measurements) to describe the directionally averaged freedom of water diffusion.

In vivo diffusion-weighted water imaging studies of prostate tissue have generally demonstrated a decrease in the measured apparent self-diffusion coefficient in prostate cancer tissue relative to normal peripheral zone glandular tissue. However, in the heterogeneous central zone assignment of diffusion characteristics to tissue type has been equivocal. Attempts to measure diffusion anisotropy in vivo have also produced equivocal results (2–8).

In vivo imaging suffers from poor spatial resolution, movement and susceptibility artifacts, and extreme difficulty in accurate correlation of imaging data with tissue type or pathologic status. Xu et al. (9) obtained reliable correlations between diffusion measurements and tissue type and pathology from a study of formalin fixed radical prostatectomy specimens. Their study, performed at 4.7 T with spatial resolution 0.5 mm × 0.5 mm × 0.5 mm, obtained diffusion anisotropy data consistent with gross tissue architecture. High FA was observed in regions of primarily fibromuscular stromal tissue with the primary diffusion axis (principle eigenvector) parallel to the assumed main fiber axis. Xu et al. suggested that the observed decrease in diffusivity in cancer relative to normal glandular tissue was consistent with: 1) the loss of large lumenal and ductal spaces (typically 100–200 μm in diameter) in which water diffusion would be expected to be relatively unrestricted relative to the intracellular and intercellular environment of packed cells and 2) increased cell density characteristic of prostatic adenocarcinoma (10).

Very high spatial resolution diffusion MRI can potentially eliminate or substantially reduce the partial volume effects that compromise the interpretation of results from lower resolution ex vivo studies of fixed tissue and in vivo studies of intact tissue. The study reported here used 16.4 T diffusion microimaging with high diffusion gradient strength to characterize the water diffusion properties of fixed prostate tissue at spatial resolution approaching the cellular scale.

MATERIALS AND METHODS

Tissue Collection

Prostate tissue was collected from radical prostatectomy specimens from three patients. The whole organs, immersed 72 h in 10% neutral buffered formalin postsurgery, were sectioned for routine histopathology. Five millimeter transverse slices were examined by a

[1]Discipline of Medical Radiation Sciences, Faculty of Health Sciences, University of Sydney, Sydney, New South Wales, Australia.

[2]Center for Advanced Imaging, University of Queensland, Brisbane, Queensland, Australia.

[3]National Imaging Facility, Queensland Node, Center for Advanced Imaging, University of Queensland, Brisbane, Queensland, Australia.

[4]Department of Urology, Royal Prince Alfred Hospital, Sydney and University of Sydney, Sydney, New South Wales, Australia.

[5]Department of Anatomical Pathology, Royal Prince Alfred Hospital, Sydney, New South Wales, Australia.

*Correspondence to: Roger Bourne, Ph.D., Discipline of Medical Radiation Sciences, Faculty of Health Sciences, University of Sydney, PO Box 170, Lidcombe, 1825, Australia. E-mail: roger.bourne@sydney.edu.au

Received 6 October 2010; revised 23 November 2010; accepted 28 November 2010.

DOI 10.1002/mrm.22778

Published online 8 February 2011 in Wiley Online Library (wileyonlinelibrary.com).

specialist urologic pathologist and tissue samples obtained with a 3-mm core punch. The selection of regions for sampling was at least 5 mm internal to the prostatic capsule and based on visual assessment of the likely tissue type. Cores were placed in vials of 10% neutral buffered formalin and stored 1–4 weeks at room temperature before MR imaging, after which the cores from the first organ were returned for histopathology. All tissue samples were collected with institutional ethics approval and written informed consent from the tissue donors.

MR Microimaging

Tissue cores were transferred from neutral buffered formalin to phosphate-buffered saline (PBS) containing 0.2% v/v gadolinium contrast agent (Magnevist, Schering AG, Germany; Dimeglumine gadopentetate 4.69 g/10 mL) and stored overnight at room temperature to wash out formaldehyde. Cores were then removed from contrast/PBS and glued (cyanoacrylate "Superglue") to a plastic strip to constrain the position of the core during imaging. The core and plastic strip were inserted into a 5 mm diameter NMR tube filled with contrast/PBS solution for imaging. The first sample (cancer tissue) was immersed in perfluorocarbon to minimize the background signal; however, after observing slight penetration of the perfluorocarbon into the tissue periphery, we desisted with its use and immersed later samples in contrast/PBS. The use of PBS also provided a background of known diffusivity and the presence of contrast agent reduced sample T_1 to ~500 msec and thus enabled shorter imaging times.

Imaging was performed on a Bruker (Germany) AV700 magnetic resonance microimaging system consisting of a 16.4 T vertical bore magnet interfaced to an AVANCE II spectrometer running Paravision 4 and using a 5 mm solenoidal radiofrequency coil. The scanner was equipped with a Micro2.5 gradient set (2.5 G/cm/A). Imaging was performed at room temperature (22°C).

For diffusion weighted imaging, a 3D spin echo diffusion tensor imaging (DTI) sequence with the following parameters was used: pulse repetition time = 500 msec, echo time = 17.9 msec, number of averages = 1, total imaging time = 14 h, field of view = 8 × 4.5 × 4.5 mm, acquisition matrix = 200 × 112 × 112 (raw data resolution = 40 × 40 × 40 μm). Diffusion parameters: $\delta = 2$ msec, $\Delta = 12$ msec, $b = 1500$ sec/mm^2 (37% gradient power), with six noncollinear directions and two $b = 0$ images.

Diffusion parameters were calculated using the program DiffusionToolkit (R. Wang and V. Wedeen, TrackVis.org, Martinos Center for Biomedical Imaging, Massachusetts General Hospital, USA; www.trackvis.org). The resulting images were displayed and analyzed with the program MIPAV (Version 0.4.4., Centre for Information Technology, NIH, USA; www.mipav.cit.nih.gov). Volume rendering was performed with MIPAV (Version 4.3.1). Voxel parameter values were measured by manual drawing of regions of interest in MIPAV. Bulk mean diffusivity was calculated as follows:

$$D = (\lambda_1 + \lambda_2 + \lambda_3)/3$$

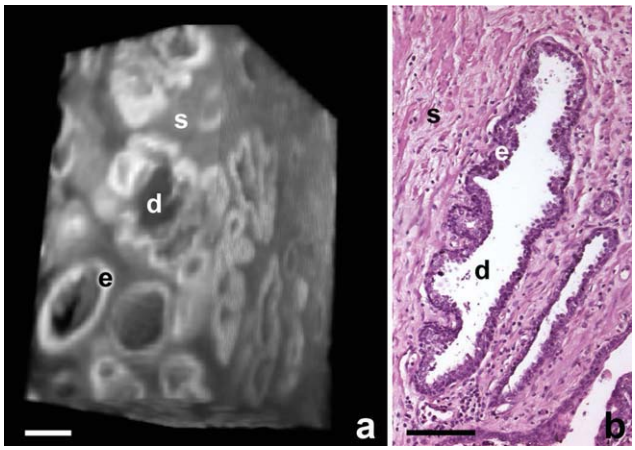

FIG. 1. Surface rendered diffusion-weighted volume image (**a**) of normal prostate tissue clearly illustrates ductal structures (d) lined with secretory epithelia (e) embedded in the stromal matrix (s). These features correspond directly with those seen on light microscopy (**b**) of normal glandular prostate tissue [not the same sample as (a)]. Three distinct diffusion compartments are apparent: ductal lumen, stromal matrix, and epithelium. Note that the epithelial cell layer is distinctly hyperintense in the diffusion-weighted image indicating highly restricted water diffusion in this layer. Scale bar =100 μm. [Color figure can be viewed in the online issue, which is available at wileyonlinelibrary.com.]

where λ_1, λ_2, and λ_3 are the eigenvalues of the diffusion tensor matrix.

Histopathology

Tissue from the first prostate was returned from imaging still glued to plastic strips. The tissue surface was marked with ink according to the MR imaging planes, carefully excised from the plastic strip, and then processed normally. The ink marking was used to embed the tissue such that sectioning planes were approximately parallel to the MR imaging planes.

RESULTS

The results presented are from a single prostate and are typical of those observed in all specimens from the three patients.

Diffusion Compartmentation

The microscopic structure of normal glandular prostate tissue is clearly visible in diffusivity images derived from diffusion-weighted microimages (Figs. 1 and 2). Three distinct diffusion compartments are apparent: ductal lumen, stromal matrix, and epithelium, and these correspond closely to the glandular architecture seen on light microscopy of the same tissue sample (Fig. 2).

In normal glandular tissue, water diffusion appears highly restricted in voxels containing the epithelial cell layer ($D = 0.4 \pm 0.1 \times 10^{-3}$ mm^2/sec). Diffusivity in the ductal lumen ($D = 2.1 \pm 0.2 \times 10^{-3}$ mm^2/sec) is similar to that observed in the contrast/PBS solution outside the tissue sample and is normal for free diffusion in water at 22°C. Intermediate diffusivity is seen in the fibromuscular stromal matrix ($D = 0.7 \pm 0.1 \times 10^{-3}$ mm^2/sec).

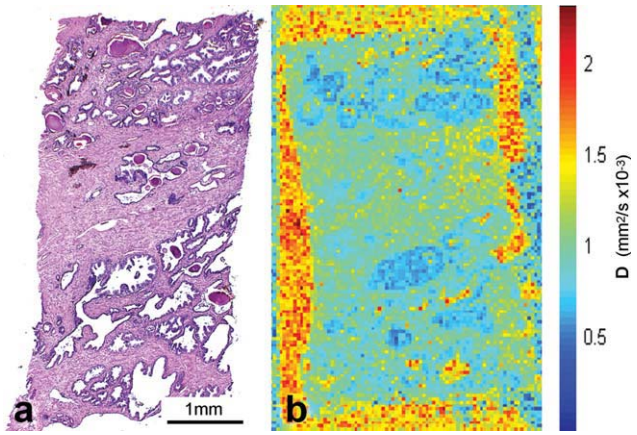

FIG. 2. Comparison of light microscopy and diffusion weighted MRI for normal peripheral zone glandular prostate tissue. **a**: Stained tissue section demonstrating normal glandular structures. **b**: Calculated diffusivity image in approximately the same tissue plane as (a). Scale bar shows units of mean diffusivity (*D*). This tissue sample was immersed in contrast/PBS.

In the tumor tissue sample (Fig. 3; Gleason pattern 4+4 adenocarcinoma), normal glandular structures were not seen in the diffusion images and the tissue has a generally low diffusivity ($D = 0.5 \pm 0.1 \times 10^{-3}$ mm^2/sec) consistent with extensive proliferation of epithelial cells and loss of ductal spaces (the diffusivity was similar in a tumor sample immersed in contrast/PBS).

Diffusion Anisotropy

As signal-to-noise ratio (SNR) was low in the high diffusivity stromal compartment an accurate estimate of FA was not possible (5). However, the average estimated FA was higher in stromal voxels than in epithelium-containing voxels of both normal glandular tissue (FA ~0.3) and tumor tissue (FA ~0.4).

DISCUSSION

This is the first report of diffusion-weighted MRI of glandular tissue with a resolution that approaches the cellular scale. The 40 μm isotropic voxel volume (~20 cell volumes) is more than three orders of magnitude smaller than that used in previous high resolution studies of prostate tissue (9,11). This very high spatial resolution permits investigation of the tissue diffusion properties with greatly reduced partial volume effects.

Diffusion Compartmentation

The diffusivities we measured are generally within the range found in the lower spatial resolution studies (0.5 mm × 0.5 mm × 0.5 mm) of formalin fixed prostate tissue by Xu et al. (9). The average voxel diffusivity in one full slice (3 mm × ~5 mm × 40 μm) of normal glandular tissue (0.7×10^{-3} mm^2/sec) was at the low end of the range Xu et al. reported for "benign peripheral zone" tissue. Allowing for partial volume effects (an estimated 20 μm thickness of a typical epithelial cell layer measured on light microcopy of H&E stained tissue), the actual diffusivity of the epithelial layer is probably not greater than 0.3×10^{-3} mm^2/sec.

A number of in vivo prostate tissue studies have demonstrated that when a large range of *b* values are measured (up to 3000 sec/mm^2) the diffusion-weighted signal shows a biexponential decay (12–14). The physical basis of the biexponential decay has been hypothesized to result from a range of factors including free and restricted diffusion compartments, exchange between such compartments, T_2 relaxation effects (15), and macromolecule binding (14). Our results strongly suggest that large differences between mean diffusivities in the ductal spaces, the epithelial cell layer, and the stromal matrix may be a major contributor to biexponential behavior observed at low spatial resolution.

Although we have identified three distinct compartments, preliminary medium resolution measurements (140 μm isotropic voxels) in fixed tissue with 16 *b* values from 0 to 1000 sec/mm^2 produced good biexponential fits with component diffusivities that cluster around *D* values of 0.4 and 0.8×10^{-3} mm^2/sec—consistent with the measured diffusivities in the epithelial and stromal compartments. Under ideal high-SNR conditions, a triexponential behavior due to signal contributions from each of the three identified compartments could be expected in normal glandular tissue.

We observed that the Gleason pattern 4+4 prostate cancer tissue sample had diffusivity lower than the mean in normal glandular tissue and intermediate between that of stromal tissue and epithelial layer. This could be the result of either the loss of high diffusivity ductal spaces and/or proliferation of epithelial cells and is consistent with the decreased high diffusivity fraction required for an optimal biexponential fit to signal decay in cancer tissue in vivo (14).

Diffusion Anisotropy

Notwithstanding the low SNR, it appears that FA is higher in stromal tissue than in the epithelial cell layer.

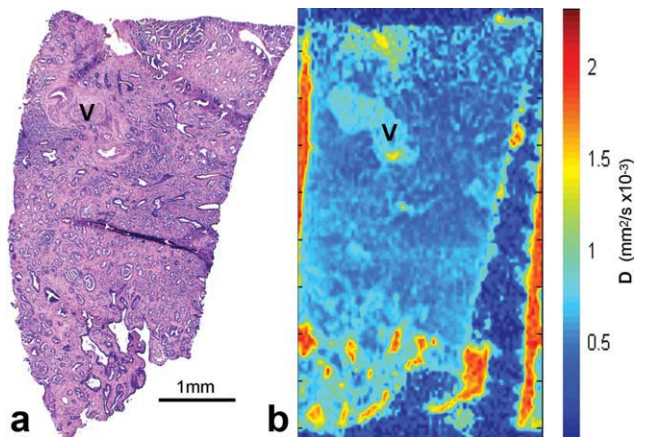

FIG. 3. Comparison of light microscopy and diffusion-weighted MRI for prostate tumor tissue. **a**: Stained tissue section demonstrating primarily Gleason pattern 4+4 adenocarcinoma. **b**: Calculated diffusivity image in approximately the same tissue plane as (a). V, vasculature. This tissue sample was immersed in perfluorocarbon. The very low *D* background represents system noise.

In this respect, our data is also consistent with the earlier low spatial resolution finding that primarily stromal regions had higher FA than regions dominated by epithelial cells (9).

Limitations

Formalin fixation, as used for tissue stabilization in this study, results in extensive crosslinking of tissue protein. The expected consequent decrease in water diffusivity relative to unfixed tissue has been previously observed in prostate tissue although relative diffusivities of different tissue types were only slightly affected (9). Although fixed tissue is a useful model for elucidation of water diffusion behavior in vivo, the three distinct compartments we observed cannot be correlated yet with any in vivo diffusion measurement. It is possible that formalin fixation creates or exaggerates a diffusion difference that is not present in fresh tissue and this requires investigation.

Although our results strongly suggest that distinct intercellular variations in water diffusivity are the most likely physical basis of biexponential diffusion behavior observed at low spatial resolution in vivo, potential contributions from other processes, including exchange between such compartments, T_2 relaxation effects (15), and macromolecule binding (14), cannot be excluded.

We achieved a b factor of 1500 sec/mm^2 with high diffusion gradient strength and a relatively short diffusion time ($\Delta = 12$ msec) to maximize SNR and minimize any T_2 contribution to diffusion contrast. The same diffusion time was used by Xu et al. in their fixed tissue studies (9). In vivo studies typically use longer diffusion times (30–50 msec) due to much lower gradient strength and may thus exhibit a greater contribution to diffusion contrast due to exchange between compartments.

CONCLUSIONS

Very high spatial resolution diffusion microimaging has demonstrated the most likely origin of biexponential diffusion decay observed in prostate MRI in vivo. Given both the close correlation between diffusion compartmentation and glandular tissue structure, and the structural definition of prostate cancer, biexponential diffusion parameter mapping may improve the sensitivity and specificity of MRI-based detection and grading of prostate cancer.

REFERENCES

1. Basser PJ, Jones DK. Diffusion-tensor MRI: theory, experimental design and data analysis—a technical review. NMR Biomed 2002;15: 456–467.
2. Kim JH, Kim JK, Park BW, Kim N, Cho KS. Apparent diffusion coefficient: prostate cancer versus noncancerous tissue according to anatomical region. J Magn Reson Imaging 2008;28:1173–1179.
3. Lim HK, Kim JK, Kim KA, Cho KS. Prostate cancer: apparent diffusion coefficient map with T2-weighted images for detection—a multireader study. Radiology 2009;250:145–151.
4. Morgan VA, Kyriazi S, Ashley SE, DeSouza NM. Evaluation of the potential of diffusion-weighted imaging in prostate cancer detection. Acta Radiol 2007;48:695–703.
5. Reinsberg SA, Brewster JM, Payne GS, Leach MO, deSouza NM. Anisotropic diffusion in prostate cancer: fact or artifact? 13th Annual Meeting of ISMRM, Miami Beach, Florida, USA. 2005.
6. Schmuecking M, Boltze C, Geyer H, Salz H, Schilling B, Wendt TG, Kloetzer KH, Marx C. Dynamic MRI and CAD vs. choline MRS: where is the detection level for a lesion characterisation in prostate cancer? Int J Radiat Biol 2009;85:814–824.
7. Haker SJ, Barnes AS, Maier SE, Tempany CM, Mulkern RV. Diffusion tensor imaging for prostate cancer detection: preliminary results from a biopsy-based assessment. 13th Annual Meeting of ISMRM, Miami Beach, Florida, USA. 2005.
8. Sinha S, Sinha U. In vivo diffusion tensor imaging of the human prostate. Magn Reson Med 2004;52:530–537.
9. Xu JQ, Humphrey PA, Kibel AS, Snyder AZ, Narra VR, Ackerman JJH, Song SK. Magnetic resonance diffusion characteristics of histologically defined prostate cancer in humans. Magn Reson Med 2009; 61:842–850.
10. Gibbs P, Liney GP, Pickles MD, Zelhof B, Rodrigues G, Turnbull LW. Correlation of ADC and T2 measurements with cell density in prostate cancer at 3.0 Tesla. Invest Radiol 2009;44:572–576.
11. Song SK, Qu ZC, Garabedian EM, Gordon JI, Milbrandt J, Ackerman JJH. Improved magnetic resonance imaging detection of prostate cancer in a transgenic mouse model. Cancer Res 2002;62:1555–1558.
12. Mulkern RV, Barnes AS, Haker SJ, Hung YP, Rybicki FJ, Maier SE, Tempany CMC. Biexponential characterization of prostate tissue water diffusion decay curves over an extended b-factor range. Magn Reson Imaging 2006;24:563–568.
13. Riches SF, Hawtin K, Charles-Edwards EM, de Souza NM. Diffusion weighted imaging of the prostate and rectal wall: comparison of biexponential and monoexponential modelled diffusion and associated perfusion coefficients. NMR Biomed 2009;22:318–325.
14. ShinMoto H, Oshio K, Tanimoto A, Higuchi N, Shigeo O, Kuribayashi S, Mulkern RV. Biexponential apparent diffusion coefficients in prostate cancer. Magn Reson Imaging 2009;27:355–359.
15. Storas TH, Gjesdal KI, Gadmar OB, Geitung JT, Klow NE. Prostate magnetic resonance imaging: multiexponential T2 decay in prostate tissue. J Magn Reson Imaging 2008;28:1166–1172.